A Sustainable Approach Using Nanocrystals Functionalized Green Alkanes as Efficient Antisolvents to Fabricate High-Quality Perovskite Films

Xiu, Jingwei; Han, Bing; Gao, Han ; Chen, Xihan; Chen, Zhenhua; Gong, Shaokuan; Yan, Xianchang; Tian, Wenming; Zhang, Xusheng; Chen, Tian; Feng, Xiyuan; Chen, Guocong; He, Dong; Deng, Yonghong; Jin, Shengye; Slater, Peter; He, Zhubing

DOI:
10.1002/aenm.202300566

A sustainable approach using nanocrystals functionalized green alkanes as efficient antisolvents to fabricate high-quality perovskite films

Jingwei Xiu,[a,b†] Bing Han,[c†], Han Gao,[a†] Xihan Chen,[d] Zhenhua Chen,[e] Shaokuan Gong,[d] Xianchang Yan,[f] Wenming Tian,[f] Xusheng Zhang,[a,b] Tian Chen,[a] Xiyuan Feng,[a] Guocong Chen,[a,b] Dong He,[a] Yonghong Deng,[a] Shengye Jin,[f] Peter Raymond Slater,[b] and Zhubing He[a,g]*

[a] Department of Materials Science and Engineering, Shenzhen Key Laboratory of Full Spectral Solar Electricity Generation (FSSEG), Southern University of Science and Technology, No. 1088, Xueyuan Rd., Shenzhen, 518055, Guangdong, China.

[b] School of Chemistry, University of Birmingham, Birmingham, B15 2TT, UK.

[c] Department of Nano Engineering, University of California San Diego, La Jolla, 92093, CA, USA

[d] SUSTech Energy Institute for Carbon Neutrality, Department of Mechanical and Energy Engineering, Southern University of Science and Technology, No. 1088, Xueyuan Rd., Shenzhen, Guangdong 518055, China

[e] Shanghai Synchrotron Facility, Shanghai Advanced Research Institute, Chinese Academy of Sciences, Shanghai, 201204, China

[f] State Key Laboratory of Molecular Reaction Dynamics and Dynamics Research Center for Energy and Environmental Materials, Dalian Institute of Chemical Physics, Chinese Academy of Sciences, Dalian 116023, China

[g] Institute of Innovative Materials (I2M), Southern University of Science and Technology, No. 1088, Xueyuan Rd., Shenzhen, 518055, Guangdong, China.

[†] J.-W. X, B. H. and H. G. contributed equally to this work.

[*] Corresponding authors: Z. H. email: hezb@sustech.edu.cn

Abstract

The industrialization of perovskite solar cells (PSCs) is approaching and demands the sustainability of their fabrication processes. To address the toxicity concern of extensively used chlorobenzene (CB) and toluene antisolvents, it is urgent to explore green and more efficient antisolvents because currently utilized green solvents lead to much lower film quality than CB. In this work, we developed a general and highly reproducible methodology of employing $CsPbI_3$ nanocrystals (NCs) functionalized green alkanes with ultralow-polarity (Alkane/NCs) as antisolvents to fabricate high-quality perovskite films. Compared with the CB processed, the perovskite films with much improved quality and high-orientation were achieved by our Alkane/NCs approach. NCs in the alkane antisolvents are proven to provide enough heterogeneous nuclei, solving effectively the discontinuous film problem encountered from using pure alkanes. Perovskite is a kind of sensitive material to electron beams, which would lose its crystallinity quickly and decompose into PbI_2 finally under traditional transmission electron microscope (TEM). Cryogenic electron microscopy (cryo-EM) is proposed to slow down the beam damage to sensitive materials, such as protein, metal organic frameworks and perovskite, during structural imaging at low temperature with low electron beam dosage. Strikingly, the lattice anchoring effect of NCs accounts for the high-orientation growth of the perovskite films as revealed directly by cryo-EM. Moreover, the phase segregation that easily occur in the CB processed perovskite film was successfully suppressed by our Alkane/NCs method. Owing to the improved film quality, the optimal device conversion efficiency was enhanced from 21.59% to 23.10% from CB to octane (OCT)/NCs. In fact, all the other alkane/NCs antisolvents involved in this work also resulted in superior device performances to CB. Impressively, the alkane/NCs processed perovskite films and their devices exhibit much improved stability over CB, with the conversion efficiency remaining at 94% of its initial value after 500 hrs light soaking for OCT/NCs device while the CB device failed around the 100 hrs. Our work clearly demonstrates the universality and reliability of the Alkane/NCs methodology, and affords a promising way to construct a green and sustainable industrialization of PSC.

Introduction

After ten years' intense study, organic-inorganic metal halides perovskite solar cells (PSC) have achieved impressive progress with the conversion efficiency surpassing 22% for large scale modules, which demonstrates that its' commercialization is approaching[1]. Inverted perovskite solar cells (IPSCs) are attractive and suitable for flexible and tandem applications. Based on the unique photophysical and electrical properties of perovskites, the efficiency of IPSC increased rapidly to 25.4% in recent years.[2] The improvement is contributed by lots of efforts in the areas, such as bulk film modification, device interfaces passivation and charge transfer layers engineering.[3] Antisolvent assisted crystallization (ASAC) is widely used for the deposition of high-quality perovskite absorber layers[4], where anti-solvents are employed to promote the nucleation of perovskites by removing such host solvents as *N,N*-Dimethylformamide (DMF) and Dimethyl sulfoxide (DMSO)[5]. As widely accepted, good anti-solvents need meet two criteria: Firstly, the anti-solvents have extremely low solubility to the perovskite compounds and therefore cannot damage the as-formed perovskite films[6]; Secondly, the anti-solvents should have certain interaction with the host solvents (e.g. DMSO) to wash out the excessive host polar solvents and herein to facilitate the nucleation of the perovskite films[6]. Currently, chlorobenzene (CB) and toluene (Tol) are the most popular anti-solvents utilized in ASAC[7]. CB and Tol are toxic and threaten human health and the environment, being damaging to the central nervous system, liver and kidney of human, as well as polluting the water, soil and atmosphere[8]. Moreover, the dose of anti-solvents used for the fabrication of PSCs are estimated to be 50-1000 ul/cm^2, which is much higher than the safety level for workers and furthermore several times the amount of hazardous host solvent used[8d]. This huge use of toxic anti-solvents severely affects the sustainability of PSCs, especially in the mass-production process. Therefore, it is urgent to explore more green and efficient anti-solvents to replace toxic CB and Tol for the target of sustainability.

To address the toxicity concern discussed above, such low-toxicity molecules as isopropanol, isobuthyl alcohol, n-butanol, ethanol, ethyl acetate, anisole, diethyl ether and etc. have been investigated as green anti-solvents[6b, 6c, 8c, 9]. Unfortunately, these green solvents result in device performances, much inferior to CB and Tol, due to their intrinsically higher polarity which would generate high nucleation density and result in

smaller grain sizes[10], and even wash out organic components in the perovskite compounds, such as FAI or MAI, and therein lead to the decomposition of the perovskites[6a, 6b, 11]. Obviously, therefore, the currently used green anti-solvents cannot replace toxic CB and Tol, and cannot meet the sustainable requirement for the future mass production of PSCs. An alternative way to boost the successful application of green anti-solvents is the engineering of NCs decorated anti-solvents. Wang et al. have reported a series of highly efficient perovskite solar cells processed with laser treated green anti-solvents, where laser was used to in-situ produce ligand-free NCs to create "anti-colloidal solution". The NCs were finally embedded in the perovskite films and helped to reduce the interfacial carrier transfer barrier, carriers recombination and boost the charge extraction at grain boundaries[12].

In fact, according to the first criterion, the polarity of anti-solvents should be as low as possible, which led to our consideration of environment-friendly alkanes. As Fig. 1a shows, such suitable alkanes as hexane (HEX), octane (OCT) and decane (DEC), have ultralow polarities in contrast to previously studied green anti-solvents and well-utilized CB. Their donor numbers (DNs) are close to 0, much lower than 2.3 of CB[13]. In principle, those alkanes are promising to overcome the problems occurring in the use of the green anti-solvents mentioned above. In the past years, some researchers reported the introduction of alkanes as additives into the above green anti-solvents to obtain dense and smooth perovskite films with larger grains by suppressing the excessive nucleation or decomposition caused by dissolution. This suggests a promising function of alkanes, although in these studies they were used as additives only[14]. Lin et al. utilized HEX as the anti-solvent to obtain a device conversion efficiency of 11.7%, which results from the ineffective removal of residual DMSO due to its weak interaction with DMSO and herein incompact films without enough nuclei[15]. The study on utilizing alkanes as anti-solvents is very rare[16], since the poor perovskite film morphology and corresponding poor device performance have dissuaded researchers from further studying alkanes as green anti-solvents despite their excellent low-polarity. Nevertheless, anti-solvent engineering of alkanes seems imperative for the sustainable mass production since PSC has run in the commercial way currently. Wang et al.

In this work, we developed a general approach of employing alkanes with different boiling points as green antisolvents to address the above issue. As a representative,

$CsPbI_3$ nanocrystals (NCs) were innovatively introduced as heterogeneous seeds to solve the insufficient homogeneous nucleation problem encountered by using pure alkanes. We call this approach as "Alkane/NCs" method. In contrast to extensively utilized CB, our Alkane/NCs method enables the growth of highly oriented and highly crystalline perovskite films. Remarkably, this approach can suppress detrimental phase segregation that easily occur in the CB processed perovskite films. Particularly, the nucleation seeds function of $CsPbI_3$ NCs is revealed to have a lattice anchoring effect by cryogenic Electron Microscopy (cryo-EM). Systematic structure analysis and optoelectronic properties characterizations provide comprehensive evidence of the power of our Alkane/NCs methodology. Owing to the improved perovskite film quality, the device conversion efficiency and stability were shown to be greatly enhanced.

Alkane-NC Methodology and Kinetic Analysis of Film Growth

The pure alkanes, HEX, OCT and DEC, were employed as green anti-solvents to prepare perovskite films, which resulted in discontinuous film morphology as shown in the Scanning Electron Microscope (SEM) images (Fig. 1b-d). This can be attributed to their weak interaction with DMSO to remove residual host solvents and therein lead to deficient nucleation[17]. To solve the issues shown from previous reports, we introduced $CsPbI_3$ NCs into the above alkane anti-solvents to induce the nucleation and growth of the perovskite films. The schematic illustration of Alkane/NCs method with (w/) and without (w/o) $CsPbI_3$ NCs for the growth of perovskite films is shown in Fig. 1e. Significantly, the grown perovskite film looks shallow brown and rough without NCs, while it becomes dark and smooth with NCs (Fig. 1f,g). The $CsPbI_3$ NCs used in this work were synthesized according to a modified hot-injection method as described in the experimental section[18]. Low and high-resolution TEM images of NCs confirm the lattice distance of 6.2 Å, which corresponds to (001) facet of cubic $CsPbI_3$ (Fig. 1h) [18]. Its' narrow photo-luminescence (PL) emitting peak at 646 nm confirms its high crystallization (Supplementary Fig. 1).[18] A typical ternary cations CsFAMA perovskite (Cesium (Cs), $HC(NH)_2^+$(FA), and $CH_3NH_3^+$(MA)) with an optical bandgap of 1.62 eV was used as the platform to examine the effect of "Alkane-NC" method while the conventional CB was taken as the control one for comparison[19]. This kind of CsFAMA perovskite has cell parameters approaching to that of the $CsPbI_3$ NCs we employed. Figure 1i shows the X-ray diffraction (XRD) patterns of perovskite films resulting from the Alkane-NC quenching approach (red) and the control of CB quenching process

(black), along with the film with pure alkane (OCT) as the anti-solvent (green). The XRD pattern of $CsPbI_3$ NCs (blue line) reveal that it has similar cell parameters to CsFAMA perovskite. The broad peaks with high-orientation of (001) facets, illustrate the nano-size nature of the NCs. Both CB and pure OCT result in perovskite films without preferred orientation. However, when $CsPbI_3$ NCs was added into OCT，the prepared perovskite film shows outstanding high-orientation with (001) facets appearing in the XRD pattern. Depending on our Alkane/NCs approach, HEX and DEC can also be utilized for the growth of high-orientation perovskite films (Supplementary Fig. 2).

The remarkably enhanced film quality led us to explore the film growth kinetic behavior of our Alkane/NCs approach. In the following kinetic analysis, OCT was chosen as the representative alkane anti-solvent. Because $CsPbI_3$ NCs were synthesized with oleylamine (OLA) as capping ligand, a little amount of OLA dissociation from $CsPbI_3$ NCs were believed to be highly likely involved into the growth of perovskite film. This can be explained by the high polarity of host solvents and the ionicity of perovskites[20]. Moreover, Zhang et al revealed the obvious influence of OLA like ligands on the growth of perovskite film[21]. Therefore，to clarify the function of OLA, we designed and synthesized the perovskite films treated by CB, OCT, OCT/NC (1mg/ml) and OCT/OLA (oleylamine, 0.1%Vol) as anti-solvents, respectively.

Firstly, we studied the intermediate wet perovskite films after spin-coating before the subsequent annealing process. Figure 2a shows the optical images of as-coated perovskite films dynamically quenched by OCT, OCT/OLA, OCT/NC and CB respectively. For OCT, the light yellow transparent as-coated film turns into a yellow and grey film after standing for 1 hour in a N_2 filled glove box. This indicates the existence of undesired yellow perovskite phase. In contrast，the other as-coated films show light brown color and turn into dark brown color finally (Fig. 2a), which indicates the dominance of cubic perovskite phase in the films. Fourier Transform Infrared (FTIR) were used to compare the amount of residual DMSO in each above wet film (Fig. 2b). The peak at 1717 cm^{-1} is assigned to be the C=N bond of FA^+, while the peak at 1020 cm^{-1} is identified as the S=O bond of DMSO[22]. When the FA^+ contents of each film are normalized, the amount of residual DMSO is the highest in the film prepared by pure OCT, which can be ascribed to the weak interaction between OCT and DMSO and the low miscibility between OCT and host solvents (Supplementary Fig. 3). Excess

residual DMSO would hinder the nucleation and growth of the perovskite films, leading to insufficient nuclei and therefore discontinuous films after thermal annealing (Fig. 1b-d). The introduction of OLA or ligands anchored NCs into anti-solvents can improve the efficiency of OCT as anti-solvent to extract DMSO out of the wet perovskite film.

Figure 2c shows the XRD patterns of the intermediate wet perovskite films after spin-coating. Strikingly, the as-coated films prepared by OCT/NCs and OCT/OLA show already highly crystalline and oriented black perovskite phase before thermal annealing, while in contrast the dominant diffraction peaks are located at 19.9° (011) for CB and OCT processed films, such that thermal annealing is necessary to drive further structure transformation into (001) oriented black phase[23]. In principle, the highly oriented and crystalline intermediate films would certainly lead to high-quality final perovskite films. δ-phase $FAPbI_3$ (11.9°, marked as "♦")[24], MAI-PbI_2-DMF adduct (13.3°, marked as "●")[25], as well as unconsumed $PbI_{2-x}Br_x$ (12.9°, marked as "*")[26], are presented in the enlarged XRD patterns as shown in Fig. 2c. Diffraction peaks belonging to δ-phase $FAPbI_3$, are present in the films from OCT, CB and OCT/OLA, while they are absent for the films from OCT/NCs. This demonstrates clearly that $CsPbI_3$ NCs can suppress the growth of the yellow phase, reinforcing the phase purity modulation effect of NCs seeds observed in former reports.[27] Strong diffraction peaks of MAI-PbI_2-DMF adduct are observed only from CB and OCT/NCs processed films. On the other hand, the strong orientation of as-coated wet films from both OCT/OLA and OCT/NCs proves unambiguously the oriented function of OLA[21]. OLA would assemble on the perovskite grains, restricting the grains' tilt during growth process and eventually resulting in a (001)-orientation-dominant wet film[21]. Here, we also investigated the optimal dose of OLA in OCT anti-solvents (Supplementary Fig. 4). A dose as low as 0.01% in volume fraction can lead to highly oriented and highly crystalline wet films, and the film quality was enhanced remarkably with the dose increasing to 0.1%. That is why the $CsPbI_3$ NCs with a little amount of capping OLA ligands can result in such high film orientation. However, further increasing the dose to 1% would be detrimental to the perovskite because of the strong Lewis base property of OLA[28]. To examine the interaction between OLA and DMSO in OCT anti-solvent, we calculated the molecular

electrostatic potential (MEP) (Fig. 2d), which has been widely used to study the intra-molecule interaction and interacting sites[6c]. The red color indicates an electron-rich area which tends to form hydrogen-bond interactions. It is interesting that the molecular structure of OLA is in the form of a surfactant, where the $–NH_2$ end site has strong negative MEP and the opposite long-chain alkanes shows very low MEP. The $-NH_2$ group at one site is favorable for the interaction with DMSO though hydrogen-bonding, while the long-chain is mutually soluble to alkanes. Therefore, OLA acts as a surfactant in OCT anti-solvent to wash out DMSO from the spin-coated wet film, which promotes the homogeneous nucleation of perovskites and then offers effective bulky nuclei sites[8c, 17c].

The above analysis demonstrates unambiguously the power of Alkane-NC methodology in modulating the quality of intermediate products. Subsequently, we characterized surface morphology and microstructure of perovskite films after thermal annealing. For OCT-only anti-solvent, the possibility of homogeneous nucleation by OCT quenching is low because of its low miscibility with host solvents and hence large-size islands form separately (Fig. 1c)[17a, 17b, 17d]. Films prepared with OCT/OLA anti-solvent show continuous film morphology with large domain size, but still with lots of pinholes and cracks both within and between the domains (Fig. 3a). As discussed above, OLA can interact with DMSO (Fig. 2d), therefore the evolution of film morphology after the introduction of OLA is realized by the removal of the remaining DMSO and increasing the nuclei number. Similar to Ostwald ripening, competitive growth would consume peripheral smaller grains, which would be responsible for the appearance of pinholes and cracks between domains (Fig. 3a)[29]. The δ-phase $FAPbI_3$ impurity in the as-coated film would also exacerbate the formation of pinholes and cracks during annealing. When using NCs, the NCs can act as nuclei seeds in heterogeneous nucleation, which is found to be more effective than the homogeneous nucleation driven by conventional antisolvents. The kinetics of NCs as heterogeneous nucleation has be explained using Gibbs free energy theory. There are two periods of growth process. The first step is the nucleation process, for which a critical free energy G* has to be overcome, the crystal grows spontaneously in the second period.[30] Heterogeneous nucleation is favorable over homogeneous nucleation during the growth of perovskite films, wherein the growth barrier is reduced at the liquid–solid interface[31]. As a result,

the addition of NCs compensates the deficiency of seeds and leads to the successful formation of a compact and dense film. Compared with the film treated by CB (Fig. 3b,c and Supplementary Fig. 5), the films prepared by OCT/NCs show larger grain size and higher orientation and better crystallinity. Our methodology is general and can be adapted to alkanes with different boiling points, such as HEX (68-70℃), OCT (125-127℃) and DEC (175℃) (Supplementary Fig. 6).

In contrast to the round grain shape of the CB processed film, the crystal-like grain morphology of the OCT/NCs film scanned by atomic force microscopy (AFM) proves the improved grain crystallinity (Fig. 3d,e). The surface roughness characterized by AFM decreases from 12 nm to 9 nm when the anti-solvent changes from CB to OCT/NCs. On the other hand, the cross-sectional SEM images (Fig. 3f,g) show vertically "wrap-through" big grains and hence illustrate again the enhanced crystallinity and the oriented growth mode of the perovskite films quenched by OCT/NCs in contrast to CB, which is favorable for carrier transport in the perovskite bulk as well. The oriented growth is further confirmed by the comparison of synchrotron-based grazing incidence wide-angle X-ray scattering (GIWAX) patterns (Fig. 3h,i), where the bolded red zones show the perpendicularly oriented growth with the function of NCs.

HRTEM characterization of perovskite films in two growth modes

Although such NCs as PVK[28], PbS[32] and carbon[33] were reported to modulate the growth of perovskite films by putting them in conventional anti-solvent or precursor.

He and Wang et al. reported a 2D covalent organic framework nanosheets induced growth method for high-quality perovskite with two-step method[34]. Systematic study of seeding agents for perovskite films has been summarized in this review[35]. However, the anchoring effect of perovskite NCs has been rarely studied and not directly evidenced. For the first time in this work we reveal the lattice interaction between NC seeds and perovskite films, which was studied by Cryo-EM. Due to the soft structure of perovskites, the electron beam in electron microscopy can damage the structure of perovskite and decompose them into PbI_2 finally[36]. In our characterization, we adopted a dose of less than 5 $e^-/Å^2$ to prevent that damage and capture the image of lattice. Figure 4a shows high resolution EM image of the CsFAMA perovskite film with a NC seed embedded in. The corresponding Fast Fourier transform (FFT) electron diffraction

of the grown perovskite film and NC show that both are present as the cubic phase (Fig 4b,c). Supplementary Figure 7 shows atomic level lattice image of the grown perovskite film via Cryo-EM, which fits well in the standard perovskite cell parameters. Regarding the lattice anchoring effect, we selected three representative areas, P1, P2 and P3 at different boundaries to study in detail (Fig 4d-f). P1 and P2 show perfect lattice matching between the same NC and the grown perovskite film (Fig. 4d,e). P3 shows a little discrepancy of 4° in the lattice mismatching between NC and the grown perovskite film (Fig. 4f), which is confirmed by its corresponding FFT electron diffraction shown in Fig. 4g. Interestingly, the mismatch at that grain boundary can shrink to 2° gradually, which may be attributed to the flexibility of perovskite structure (Fig. 4a). Therefore, the NC interlinks the adjacent matrix perovskite crystals together and the strong lattice anchoring behavior drives them to grow in identical orientations. In contrast, the lattice mismatch can reach over 20° at the grain boundaries in the routinely grown perovskite film by CB (Fig. 4h). The enlarged HRTEM image of grain boundaries of the routinely grown perovskite is presented in Supplementary Fig. 8, which shows random orientation and coincides with the growth mode conclusion drawn above. This remarkable comparison reveals for the first time the unique lattice anchoring function of NCs visually and provides answers to the different growth modes between OCT/NCs and CB antisolvents, especially shown in the XRD patterns in Figs. 1i and 2c.

Optoelectronic properties investigation

After comparing the difference between perovskite films prepared by OCT/NCs and CB, we investigated their optoelectronic properties by means of spectroscopy tools. Figure 5a shows their normalized absorption and photoluminescence (PL) spectra. Their absorption edges are determined at 765 nm and 1.62 eV deduced by their correspondent Tauc plot (Supplementary Fig. 9). This optical band gap value coincides with their PL emission peaks at 760 nm. However, their difference is a wide absorption bump from 780nm to 850nm and a small and extra PL emission peaks around 845 nm shown as the inset in Fig. 5a for CB processed perovskite film. This difference indicates the existence of phase segregation in the perovskite film prepared with CB, and the segregation of OCT/NCs film was much reduced. This drove us to look into their magnified XRD patterns (Fig. 5b). In contrast to the OCT/NCs film, the film prepared with CB shows a split diffraction at (211) facet around 35°, which demonstrates the occurrence of phase segregation in the CB film. By investigating the intermediate wet

perovskite films (Supplementary Fig. 10), the phase segregation has already taken place before thermal annealing for the film prepared with CB. The phase segregation is likely to be FA^+/I^- rich phase, evidenced by the lower band gap of the new phase[37]. This result is also coincident with the appearance of δ-phase $FAPbI_3$ segregation in the as-coated film discussed in Fig 2c. In this work, this phase segregation is successfully suppressed by our OCT/NCs method. Temperature-dependent and time-resolved photo-luminescence (TRPL) was conducted with the raw data shown in Supplementary Fig. 11. In contrast to OCT/NCs, the sharp decline of lifetime in the TRPL kinetics of the CB film indicates higher defect densities, which is consistent with the conclusion drawn above. The CB film shows an almost linear decline from 886 ns to 66 ns when the temperature increases from 120K to 300K, whereas, the OCT/NCs film shows a different trace with a kink point at 220K (Fig. 5c). Below 220K, the tetragonal phase dominates and the lifetime decreases when the temperature increases resulting from the meeting of thermal activation for phonon scattering and trap sites[38]. Above 220K, the rebound in lifetimes results from the changing rotational motion of organic molecule by phase transformation from tetragonal to cubic phase[39]. However, the PL lifetime of the CB film keeps declining, which indicates the traps dominate the variation of lifetime because the trap density is much higher than that in the OCT/NCs film.

Besides the bulk quality of film, the interfacial trap density also influences its optoelectronic properties and herein device performance. Transient reflection spectroscopy (TR) was employed to investigate the NiO/PVK interface. It is apparent that the CB film has an extra reflection signal around 660 nm besides the intrinsic reflection at ca. 750 nm (Fig. 5d), while the extra absorption of the OCT/NCs film is negligible (Fig. 5e). The 660nm-site absorption at the NiO/PVK interface of the CB film can be ascribed to Br^- rich wide band gap perovskites segregated at the interface which is verified by the element profile across the film by means of in-depth XPS measurements (Supplementary Fig. 12). In Fig. 5f, the etch time dependent Br^-/I^- composition ratio can clearly demonstrate the higher concentration of Br^- at the interface of the NiO/ITO side in the CB processed perovskite film. The segregation of wide band gap perovskite mainly happens at the NiO/PVK surface, so that the signal belonging to the wide band perovskite is absent in transient absorption (TA) both for CB and OCT/NCs processed perovskite (Supplementary Fig. 13). The lifetime exhibits a slight increase from CB to OCT/NCs processed samples (Fig. 5g).

We also conducted surface carrier kinetics measured with transient reflection, excited with 2.58 eV (480 nm), 2.07 eV (600 nm) and 1.65 eV (750 nm) pump pulses (Fig. 5h,i). By simultaneously modeling the decay of the charge carriers with a global fitting procedure that includes both diffusion and surface extraction, the best-fit values were obtained as shown Supplementary Table 1. The OCT/NCs processed perovskite film shows higher diffusion coefficient (0.4950 ± 0.0524 cm^2/s vs 0.0265 ± 0.0042 cm^2/s), which proves the high quality of bulk film, while the obtained higher surface extraction velocity (2.31 ± 1.07m/s vs 1.37 ± 0.53 m/s) indicates efficient hole extraction at the NiO/perovskite interface.

Device performance and device physics analysis

Figure 6a shows the performance distribution of devices fabricated by using different pure alkanes and alkane/NCs as anti-solvents. The devices with pure alkanes as anti-solvents show ultralow conversion efficiencies, resulting from their derived discontinuous perovskite films (Fig. 1b-d). Benefiting from preferred orientation, suppressed phase segregation and smooth perovskite surface, the devices based on the Alkane/NCs processed perovskite films, exhibit performance better than CB processed devices. The best CB device achieved a conversion efficiency of 21.59% with V_{oc}=1.18 V, J_{sc}=22.9 mA/cm^2, and FF=79.9% (Fig. 6b). In comparison, the optimal OCT/NCs device achieved the PCE of 23.1% with V_{oc}=1.18 V, J_{sc}=23.3 mA/cm^2, and FF=84.1%. Moreover, OCT/NCs processed devices show an average efficiency of 22.2%. The improvement of efficiency is boosted by the factor of current density and fill factor (Supplementary Fig. 14). The enhancement of J_{sc} is confirmed by EQE measurement, where the integrated current density increases from 21.5 mA/cm^2 to 22.2 mA/cm^2 (Supplementary Fig. 15). In fact, along with OCT/NCs, HEX/NCs and DEC/NCs also obtained the device performance superior to CB (Fig. 6a). To understand the charge recombination and transport in devices, we conducted transient photovoltage (TPV) and transit photo-current (TPC) measurements by irradiating the devices with a pulsed laser under the open-circuit and the short-circuit conditions. The recombination lifetimes deduced from the TPV decay curves for the devices fabricated by CB and OCT/NCs are 0.74 ms and 0.9 ms, respectively, indicating the suppressed trap centers in the OCT/NCs device (Fig. 6c), which is consistent with its superior carrier lifetime

discussed above and shown in Fig. 5g. Charge extraction time can be derived from the TPC decay curves (Fig. 6d). The charge extraction time for the devices fabricated by CB and OCT/NC are 0.5 μs and 0.24 μs, respectively. The faster charge extraction confirms the enhanced perovskite film quality by OCT/NCs, especially embodied at the interfaces, which coincides with the TA results discussed in Fig. 5h,i and Supplementary Table 1. Moreover, the recombination resistance (R_{rec}) extracted from the electrochemical impedance spectroscopy (EIS)[56], increases from 1.6 KΩ to 2.3 KΩ (Supplementary Fig. 16), which further supports the suppressed defect density and improved quality of perovskite films by use of OCT/NCs.

Then, we investigated the long-term device stability via maximal power point tracking (MPPT) measurements in ambient environment at one standard sun irradiation for their encapsulated devices (Fig. 6e). The OCT/NCs device show much improved stability with the conversion efficiency remaining 94% of its initial value after 500 hrs light soaking for OCT/NCs devices while the CB device failed around 100 hrs. We also conducted XRD measurements to study the stability of the perovskite layers under high temperature (100 °C) and high environmental moisture (60%-80% RH) (Supplementary Fig. 17). As a result, the signal of $PbBr_xI_{2-x}$ at 12.9º in the CB processed perovskite films becomes stronger and gradually dominates in the XRD pattern with a heating duration of 6 hrs while the OCT/NCs film exhibits negligible variation, especially regarding the phase segregation, this illustrating excellent stability (Supplementary Fig. 18). When exposed to ambient environment with a humidity between 60%-80% RH up to 48h, similar differences were seen, which clearly illustrates the excellent perovskite film quality produced by our OCT/NCs methodology. The improvement of humidity stability is not only related to the crystallinity of perovskite film, but also resulted from the hydrophobicity of long-chain oleylamine and oleic acid ligands from NCs as evidenced in previous literature.[40]

Conclusion

In summary, we report a general and sustainable methodology with green alkane/NCs as antisolvent in the fabrication process of PSCs, to address the toxicity concerns of extensively utilized CB. Whereas with so ultralow DN and polarity, alkanes with suitable boiling points cannot wash out residual host solvent such as DMSO from the spin-coated wet perovskite film or provide enough homogeneous nuclei for the growth of continuous film, due to lacking favorable interaction with DMSO. Through

systematic structure characterizations, NCs along with their OLA ligands in the alkanes antisolvents are proven to solve these issues, by providing enough heterogeneous nuclei for the growth of compact perovskite films. Strikingly, we are able to observe the lattice anchoring effect of NCs for the high-orientation growth of perovskite films directly by cryo-EM. Phase segregations were shown to easily occur in the conventional CB processed perovskite film as illustrated by steady-state and transient optoelectronic spectroscopies and in-depth XPS, which is ascribed to the composition precipitation of FA^+/I^- rich in the bulk and Br^- rich at the interface of NiO/PVK. In contrast, those phase segregations were successfully suppressed by our novel Alkane/NCs method and the film quality is much improved in contrast to the CB processed. Owing to the improved film quality, the device conversion efficiency was enhanced from 21.59% to 23.10% from CB to OCT/NCs. In fact, all the other alkane/NCs antisolvents studied in this work also led to device performances superior to CB. Impressively, the alkane/NCs processed perovskite films and their based devices also exhibited much improved stability over CB, with the conversion efficiency remaining 94% of its initial value after 500 hrs light soaking for OCT/NCs devices while the CB device failed around 100 hrs. Our Alkane/NCs methodology therefore unambiguously paves an extremely promising new approach to constructing a green and sustainable process for the industrialization of PSC.

Acknowledgements

This work was supported by the National Natural Science Foundation of China (NSFC) (Nos. U2001216, 52273266) and the Shenzhen Key Laboratory Project (No. ZDSYS201602261933302) from the Science, Technology and Innovation Commission of Shenzhen Municipality. The authors thank the Core Research Facilities, Cryogenic Electronic Microscopy Center and Department of Materials Science and Engineering of SUSTech for the characterizations in this work.[12a]

Author contributions

Z.H. conceived and supervised the project. J.-W.X. conceived the idea, designed and conducted the experiments. H.G. synthesized $CsPbI_3$ NCs and carried out some characterizations of XRD and SEM. B.H. and D.H. performed Cryo-EM and analyzed the data along with Y.-H.D.. X.-C.Y., W.-M.T. and S.-Y.J. carried out temperature-

dependent PL and TRPL measurements. X.-S.Z. carried out FTIR measurement. X.-H.C. and S.-K.G. carried out TA and TR measurements. Z.-H.C. conducted GIWAX measurement. T.C. X.-Y. F. and G.-C.C. contributed to the device fabrications and characterizations. P.-R.S. discussed and directed experiments. J.-W.X. and Z.H. wrote the paper. All authors reviewed the manuscript.

Interests of Conflict

The authors declare no conflicting interests.

References

[1] a)Z. Saki, M. M. Byranvand, N. Taghavinia, M. Kedia, M. Saliba, *Energy & Environmental Science* **2021**, 14, 5690; b)L. Chu, S. Zhai, W. Ahmad, J. Zhang, Y. Zang, W. Yan, Y. Li, *Nano Research Energy* **2022**, 1, e9120024; c)J. Tang, L. Liu, Z. Yu, J. Du, X. Cai, M. Zhang, M. Zhao, L. Bai, Z. Gai, S. Cui, *Advanced Sustainable Systems* **2022**, 6, 2100510; d)F. Wu, S. Lu, C. Hu, H. Lu, C. Chen, J. Tang, S. Yang, L. Zhu, *Advanced Sustainable Systems* **2022**, 6, 2200212; e)W. Liu, H. Raza, X. Hu, S. Liu, Z. Liu, W. Chen, *Materials Futures* **2023**, 2, 012103.

[2] R. Garai, M. A. Afroz, R. K. Gupta, P. K. Iyer, *Advanced Sustainable Systems* **2020**, 4, 2000078.

[3] a)S. Wang, M.-H. Li, Y. Jiang, J.-S. Hu, *Materials Futures* **2023**, 2, 012102; b)D. Li, Y. Huang, Z. Ren, A. Amini, A. B. Djurišić, C. Cheng, G. Li, *Journal of Energy Chemistry* **2023**, 79, 168.

[4] a)H.-S. Kim, Y.-J. An, J. I. Kwak, H. J. Kim, H. S. Jung, N.-G. Park, *ACS Energy Letters* **2022**, 7, 1154; b)M. Xiao, F. Huang, W. Huang, Y. Dkhissi, Y. Zhu, J. Etheridge, A. Gray‐Weale, U. Bach, Y. B. Cheng, L. Spiccia, *Angewandte Chemie International Edition* **2014**, 53, 9898; c)X. Wang, Y. Xu, H. Zhang, Z. Yan, Y. Jing, X. Liu, J. Wu, Z. Lan, *Advanced Sustainable Systems* **2022**, 6, 2200074.

[5] a)S. Tan, T. Huang, I. Yavuz, R. Wang, T. W. Yoon, M. Xu, Q. Xing, K. Park, D.-K. Lee, C.-H. Chen, *Nature* **2022**, 605, 268; b)M. Zhang, Z. Wang, B. Zhou, X. Jia, Q. Ma, N. Yuan, X. Zheng, J. Ding, W. H. Zhang, *Solar Rrl* **2018**, 2, 1700213.

[6] a)M. T. Hoang, F. Ünlü, W. Martens, J. Bell, S. Mathur, H. Wang, *Green Chemistry* **2021**, 23, 5302; b)T. Bu, L. Wu, X. Liu, X. Yang, P. Zhou, X. Yu, T. Qin, J. Shi, S. Wang, S. Li, *Advanced Energy Materials* **2017**, 7, 1700576; c)W. Zhang, Y. Li, X. Liu, D. Tang, X. Li, X. Yuan, *Chemical Engineering Journal* **2020**, 379, 122298.

[7] a)Z. Li, B. Li, X. Wu, S. A. Sheppard, S. Zhang, D. Gao, N. J. Long, Z. Zhu, *Science* **2022**, 376, 416; b)Q. Jiang, J. Tong, Y. Xian, R. A. Kerner, S. P. Dunfield, C. Xiao, R. A. Scheidt, D. Kuciauskas, X. Wang, M. P. Hautzinger, *Nature* **2022**, 611, 278; c)R. Lin, J. Xu, M. Wei, Y. Wang, Z. Qin, Z. Liu, J. Wu, K. Xiao, B. Chen,

S. M. Park, *Nature* **2022**, 603, 73; d)M. Yang, Z. Li, M. O. Reese, O. G. Reid, D. H. Kim, S. Siol, T. R. Klein, Y. Yan, J. J. Berry, M. F. Van Hest, *Nature Energy* **2017**, 2, 17038.

[8] a)L. Wang, X. Wang, L.-L. Deng, S. Leng, X. Guo, C.-H. Tan, W. C. Choy, C.-C. Chen, *Materials Horizons* **2020**, 7, 934; b)Y. Yun, F. Wang, H. Huang, Y. Fang, S. Liu, W. Huang, Z. Cheng, Y. Liu, Y. Cao, M. Gao, *Advanced Materials* **2020**, 32, 1907123; c)W. Xu, Y. Gao, W. Ming, F. He, J. Li, X. H. Zhu, F. Kang, J. Li, G. Wei, *Advanced Materials* **2020**, 32, 2003965; d)S. Ghosh, S. Mishra, T. Singh, *Advanced Materials Interfaces* **2020**, 7, 2000950.

[9] a)M. Yavari, M. Mazloum‐Ardakani, S. Gholipour, M. M. Tavakoli, S. H. Turren‐Cruz, N. Taghavinia, M. Grätzel, A. Hagfeldt, M. Saliba, *Advanced Energy Materials* **2018**, 8, 1800177; b)X. Wang, Z. Han, F. Gao, C. Luo, Q. Zhao, *Solar RRL* **2022**, 6, 2100973.

[10] a)Y. Zhou, M. Yang, W. Wu, A. L. Vasiliev, K. Zhu, N. P. Padture, *Journal of Materials Chemistry A* **2015**, 3, 8178; b)N. J. Jeon, J. H. Noh, Y. C. Kim, W. S. Yang, S. Ryu, S. I. Seok, *Nature materials* **2014**, 13, 897.

[11] F. Zhang, J. Lian, J. Song, Y. Hao, P. Zeng, H. Niu, *Journal of Materials Chemistry A* **2016**, 4, 3438.

[12] a)P. Guo, C. Liu, X. Li, Z. Chen, H. Zhu, L. Zhu, X. Zhang, W. Zhao, N. Jia, Q. Ye, H. Wang, *Advanced Energy Materials* **2022**, 2202395; b)H. Yu, W. Zhao, L. Ren, H. Wang, P. Guo, X. Yang, Q. Ye, D. Shchukin, Y. Du, S. Dou, *Advanced Materials* **2020**, 32, 2001571; c)P. Guo, X. Yang, Q. Ye, J. Zhang, H. Wang, H. Yu, W. Zhao, C. Liu, H. Yang, H. Wang, *Advanced Energy Materials* **2019**, 9, 1901341; d)P. Guo, H. Zhu, W. Zhao, C. Liu, L. Zhu, Q. Ye, N. Jia, H. Wang, X. Zhang, W. Huang, *Advanced Materials* **2021**, 33, 2101590.

[13] a)A. Marzec, M. Juzwa, K. Betlej, M. Sobkowiak, *Fuel Processing Technology* **1979**, 2, 35; b)V. Gutmann, *Coordination Chemistry Reviews* **1976**, 18, 225.

[14] H. B. Lee, M. K. Jeon, N. Kumar, B. Tyagi, J. W. Kang, *Advanced Functional Materials* **2019**, 29, 1903213.

[15] N. Lin, J. Qiao, H. Dong, F. Ma, L. Wang, *Journal of Materials Chemistry A* **2015**, 3, 22839.

[16] D. Y. Heo, W. J. Jang, M. J. Jeong, J. H. Noh, S. Y. Kim, *Solar RRL* **2022**, 6, 2200485.

[17] a)W. Nie, H. Tsai, R. Asadpour, J.-C. Blancon, A. J. Neukirch, G. Gupta, J. J. Crochet, M. Chhowalla, S. Tretiak, M. A. Alam, *Science* **2015**, 347, 522; b)M. He, B. Li, X. Cui, B. Jiang, Y. He, Y. Chen, D. O'Neil, P. Szymanski, M. A. Ei-Sayed, J. Huang, *Nature communications* **2017**, 8, 1; c)C. Liu, Y.-B. Cheng, Z. Ge, *Chemical Society Reviews* **2020**, 49, 1653; d)Y. Deng, E. Peng, Y. Shao, Z. Xiao, Q. Dong, J. Huang, *Energy & Environmental Science* **2015**, 8, 1544.

[18] A. Swarnkar, A. R. Marshall, E. M. Sanehira, B. D. Chernomordik, D. T. Moore, J. A. Christians, T. Chakrabarti, J. M. Luther, *Science* **2016**, 354, 92.

[19] Q. Hu, W. Chen, W. Yang, Y. Li, Y. Zhou, B. W. Larson, J. C. Johnson, Y.-H. Lu, W. Zhong, J. Xu, *Joule* **2020**, 4, 1575.

[20] J. Li, L. Xu, T. Wang, J. Song, J. Chen, J. Xue, Y. Dong, B. Cai, Q. Shan, B. Han, *Advanced materials* **2017**, 29, 1603885.

[21] X. Zheng, Y. Hou, C. Bao, J. Yin, F. Yuan, Z. Huang, K. Song, J. Liu, J. Troughton, N. Gasparini, *Nature Energy* **2020**, 5, 131.

[22] Z. Yang, W. Zhang, S. Wu, H. Zhu, Z. Liu, Z. Liu, Z. Jiang, R. Chen, J. Zhou, Q. Lu, *Science Advances* **2021**, 7, eabg3749.

[23] X. Han, H. Xiong, J. Qi, Y. Rui, X. Zhang, C. Hou, Y. Li, H. Wang, Q. Zhang, *Solar Energy* **2019**, 186, 225.

[24] a)K. Poorkazem, T. L. Kelly, *Sustainable Energy & Fuels* **2018**, 2, 1332; b)F. Yang, L. Dong, D. Jang, K. C. Tam, K. Zhang, N. Li, F. Guo, C. Li, C. Arrive, M. Bertrand, *Advanced Energy Materials* **2020**, 10,

2001869; c)F. Xie, C.-C. Chen, Y. Wu, X. Li, M. Cai, X. Liu, X. Yang, L. Han, *Energy & Environmental Science* **2017**, 10, 1942.
[25] A. A. Petrov, N. Pellet, J.-Y. Seo, N. A. Belich, D. Y. Kovalev, A. V. Shevelkov, E. A. Goodilin, S. M. Zakeeruddin, A. B. Tarasov, M. Graetzel, *Chemistry of Materials* **2017**, 29, 587.
[26] M. Saliba, T. Matsui, K. Domanski, J.-Y. Seo, A. Ummadisingu, S. M. Zakeeruddin, J.-P. Correa-Baena, W. R. Tress, A. Abate, A. Hagfeldt, *Science* **2016**, 354, 206.
[27] H.-Q. Xu, K. Wang, M. Ding, D. Feng, H.-L. Jiang, H.-C. Zhou, *Journal of the American Chemical Society* **2016**, 138, 5316.
[28] W. Yang, R. Su, D. Luo, Q. Hu, F. Zhang, Z. Xu, Z. Wang, J. Tang, Z. Lv, X. Yang, *Nano Energy* **2020**, 67, 104189.
[29] a)Y. Fu, F. Meng, M. B. Rowley, B. J. Thompson, M. J. Shearer, D. Ma, R. J. Hamers, J. C. Wright, S. Jin, *Journal of the American Chemical Society* **2015**, 137, 5810; b)H. Chen, Z. Wei, H. He, X. Zheng, K. S. Wong, S. Yang, *Advanced Energy Materials* **2016**, 6, 1502087; c)B. Li, Y. Zhang, L. Fu, T. Yu, S. Zhou, L. Zhang, L. Yin, *Nature communications* **2018**, 9, 1.
[30] Y. Zhao, H. Tan, H. Yuan, Z. Yang, J. Z. Fan, J. Kim, O. Voznyy, X. Gong, L. N. Quan, C. S. Tan, *Nature communications* **2018**, 9, 1.
[31] a)S.-S. Li, C.-H. Chang, Y.-C. Wang, C.-W. Lin, D.-Y. Wang, J.-C. Lin, C.-C. Chen, H.-S. Sheu, H.-C. Chia, W.-R. Wu, *Energy & Environmental Science* **2016**, 9, 1282; b)J. W. Gibbs, *Trans Connecticut Acad* **1967**.
[32] Z. Ning, X. Gong, R. Comin, G. Walters, F. Fan, O. Voznyy, E. Yassitepe, A. Buin, S. Hoogland, E. H. Sargent, *Nature* **2015**, 523, 324.
[33] a)S. Li, Z. He, Y. Li, K. Liu, M. Chen, Y. Yang, X. Li, *Journal of Alloys and Compounds* **2021**, 889, 161561; b)Y. Rui, Z. Jin, X. Fan, W. Li, B. Li, T. Li, Y. Wang, L. Wang, J. Liang, *Materials Futures* **2022**, 1, 045101.
[34] a)J. He, H. Liu, F. Zhang, X. Li, S. Wang, *Advanced Functional Materials* **2022**, 32, 2110030; b)S. Chen, X. Xiao, B. Chen, L. L. Kelly, J. Zhao, Y. Lin, M. F. Toney, J. Huang, *Science Advances* **2021**, 7, eabb2412.
[35] J. He, S. Wang, X. Li, F. Zhang, *ChemSusChem* **2023**, e202202109.
[36] Y. Li, W. Zhou, Y. Li, W. Huang, Z. Zhang, G. Chen, H. Wang, G.-H. Wu, N. Rolston, R. Vila, *Joule* **2019**, 3, 2854.
[37] a)S. G. Motti, J. B. Patel, R. D. Oliver, H. J. Snaith, M. B. Johnston, L. M. Herz, *Nature communications* **2021**, 12, 1; b)W. Yang, H. Long, X. Sha, J. Sun, Y. Zhao, C. Guo, X. Peng, C. Shou, X. Yang, J. Sheng, *Advanced Functional Materials* **2022**, 32, 2110698; c)Y. Wang, X. Guan, W. Chen, J. Yang, L. Hu, J. Yang, S. Li, K. Kalantar-Zadeh, X. Wen, T. Wu, *ACS applied materials & interfaces* **2020**, 12, 38376.
[38] a)H. C. Woo, J. W. Choi, J. Shin, S.-H. Chin, M. H. Ann, C.-L. Lee, *The journal of physical chemistry letters* **2018**, 9, 4066; b)S. Kahmann, O. Nazarenko, S. Shao, O. Hordiichuk, M. Kepenekian, J. Even, M. V. Kovalenko, G. R. Blake, M. A. Loi, *ACS Energy Letters* **2020**, 5, 2512.
[39] T. Chen, W.-L. Chen, B. J. Foley, J. Lee, J. P. Ruff, J. P. Ko, C. M. Brown, L. W. Harriger, D. Zhang, C. Park, *Proceedings of the National Academy of Sciences* **2017**, 114, 7519.
[40] a)J. Ye, M. M. Byranvand, C. O. Martínez, R. L. Hoye, M. Saliba, L. Polavarapu, *Angewandte Chemie* **2021**, 133, 21804; b)I. Poli, X. Liang, R. Baker, S. Eslava, P. J. Cameron, *Journal of Materials Chemistry C* **2018**, 6, 7149.

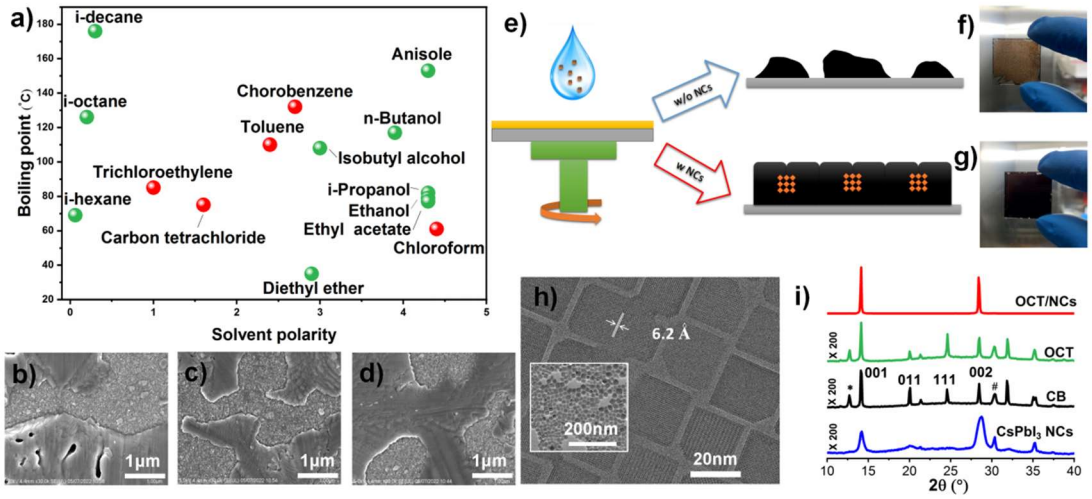

Fig. 1 | Illustration of "Alkane-NC" method for the preparation high-quality perovskite films. a, Diagram of boiling point versus polarity of anti-solvents. **b-d,** Scanning Electron Microscope images of perovskite films dripped by pure (**b**) HEX (**c**) OCT and (**d**) DEC as anti-solvents. **e,** Demonstration of perovskite films fabricated by alkanes w/o and w/ $CsPbI_3$ NCs. **f,g,** Optical photos of perovskite films fabricated by octane (**f**) w/o and (**g**) w/ $CsPbI_3$ NCs. **h,** Transmission Electron Microscope and high-solution Transmission Electron Microscope images of $CsPbI_3$ NCs. Scale bar: 20 nm (inset 100nm). **i,** X-ray diffraction patterns of $CsPbI_3$ NCs, perovskite films processed with CB, OCT and OCT with $CsPbI_3$ NCs. (*: $PbI_{2-x}Br_x$, #: ITO)

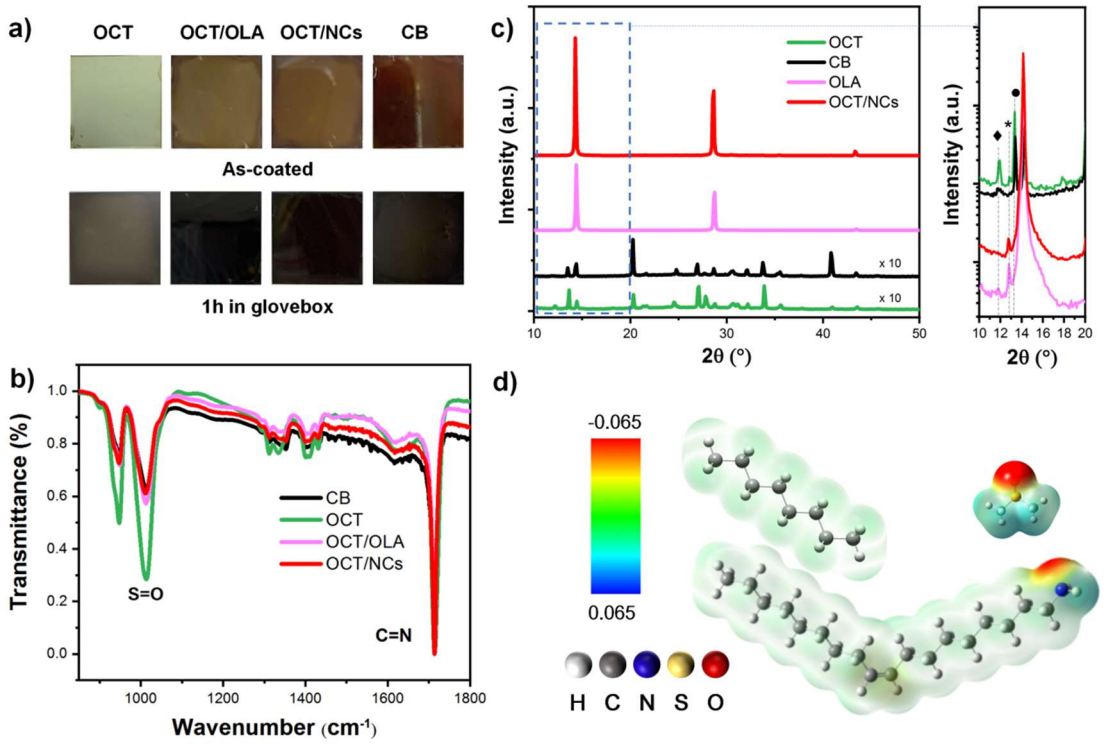

Fig. 2 | Characterization of as-coated wet perovskite films. a, Optical photographs of as-coated wet films before and after standing in N_2 glove box for 1h at room-temperature. **b,** Corresponding Fourier Transform Infrared spectra. **c,** XRD patterns of as-coated film (left). The detail of patterns ranged from 10° to 20° (right). **d,** The molecular electrostatic potential of OLA and an illustration of interaction between OLA, DMSO and OCT.

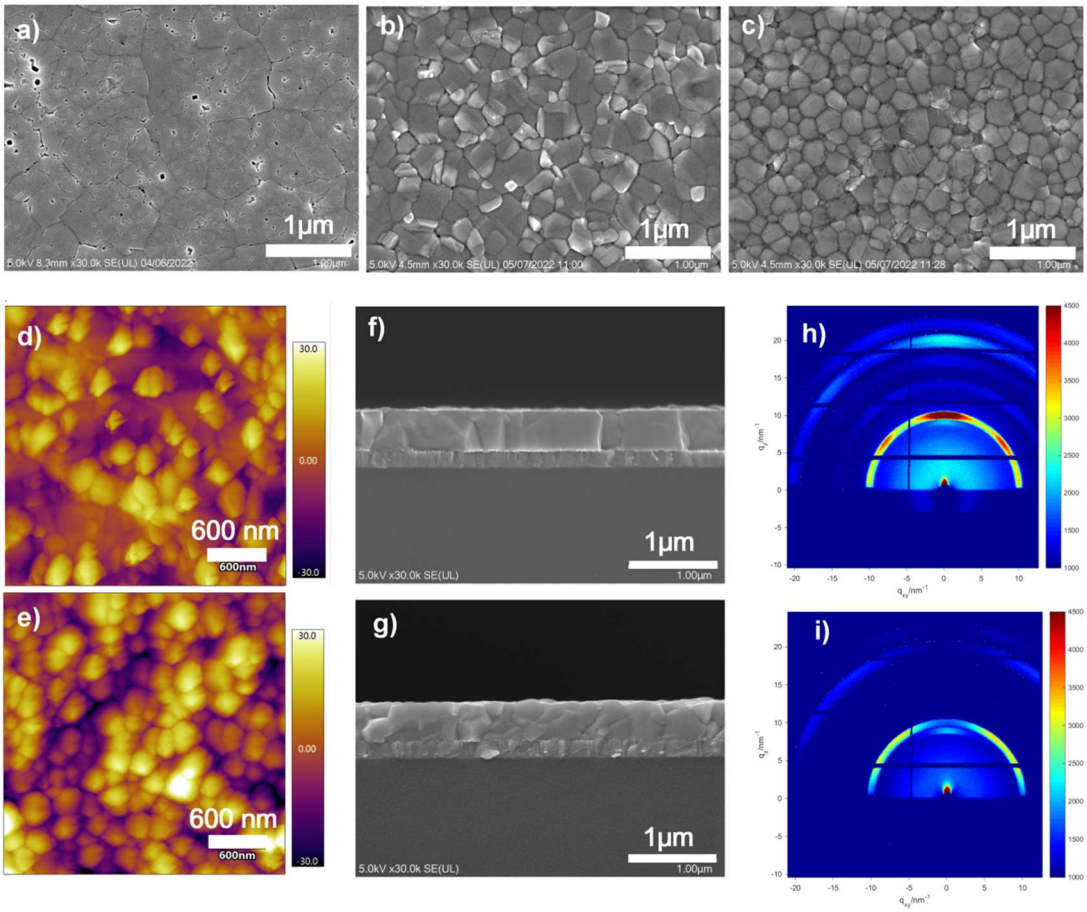

Fig. 3 | Characterization of annealed perovskite films. a-c, SEM images of (**a**) OCT/OLA, (**b**) OCT/NCs and (**c**) CB processed perovskite films. **d,e,** AFM images of (**d**) OCT/NCs and (**e**) CB processed perovskite films. **f,g,** Cross-section Scanning Electron Microscope images of (**f**) OCT/NCs and (**g**) CB processed perovskite films. **h,i,** GIWAX of (**h**) OCT/NCs and (**i**) CB processed perovskite films.

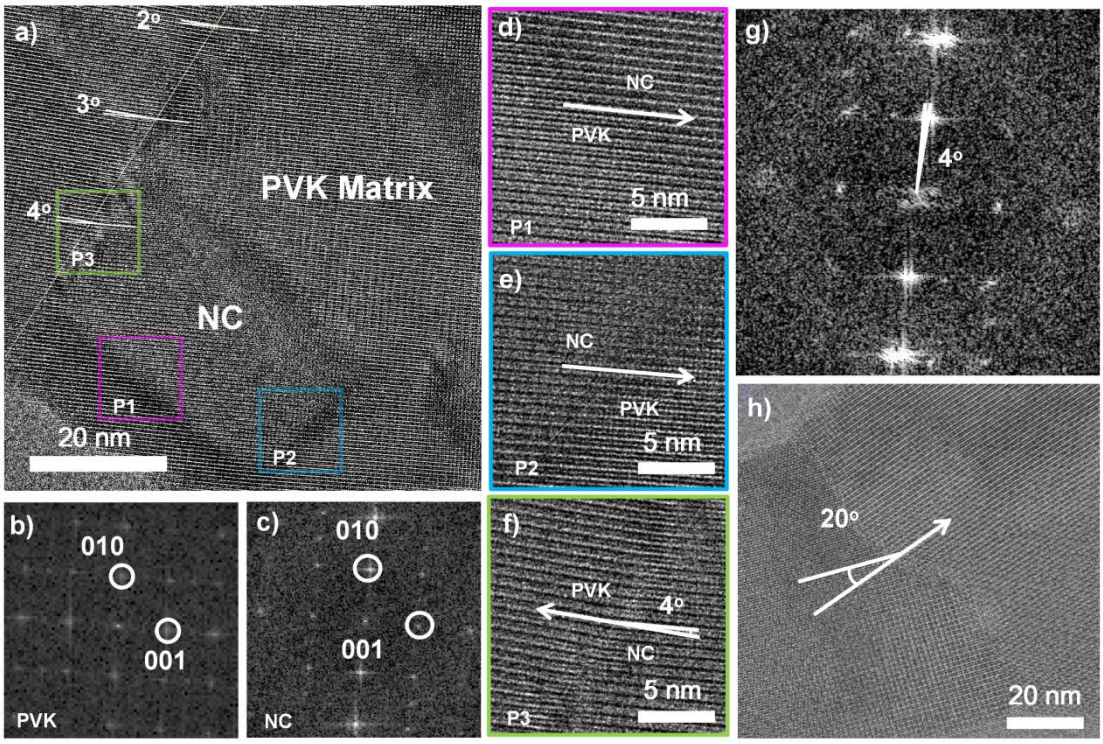

Fig. 4 | Cryo-EM Characterization. a, High-resolution transmission electron microscopy (HRTEM) images of a $CsPbI_3$ NC embed in CsFAMA perovskite. **b,c,** Fast Fourier transform of HRTEM images corresponding to the area of (**b**) CsFAMA perovskite and (**c**) $CsPbI_3$ NC. **d-f,** HRTEM images of grain boundary between CsFAMA perovskite and NC corresponding to the areas of (**d**) P1, (**e**) P2, (**f**) P3. **g,** Fast Fourier transform of HRTEM images of P3. H) HRTEM image of grain boundary in perovskite prepared without NCs.

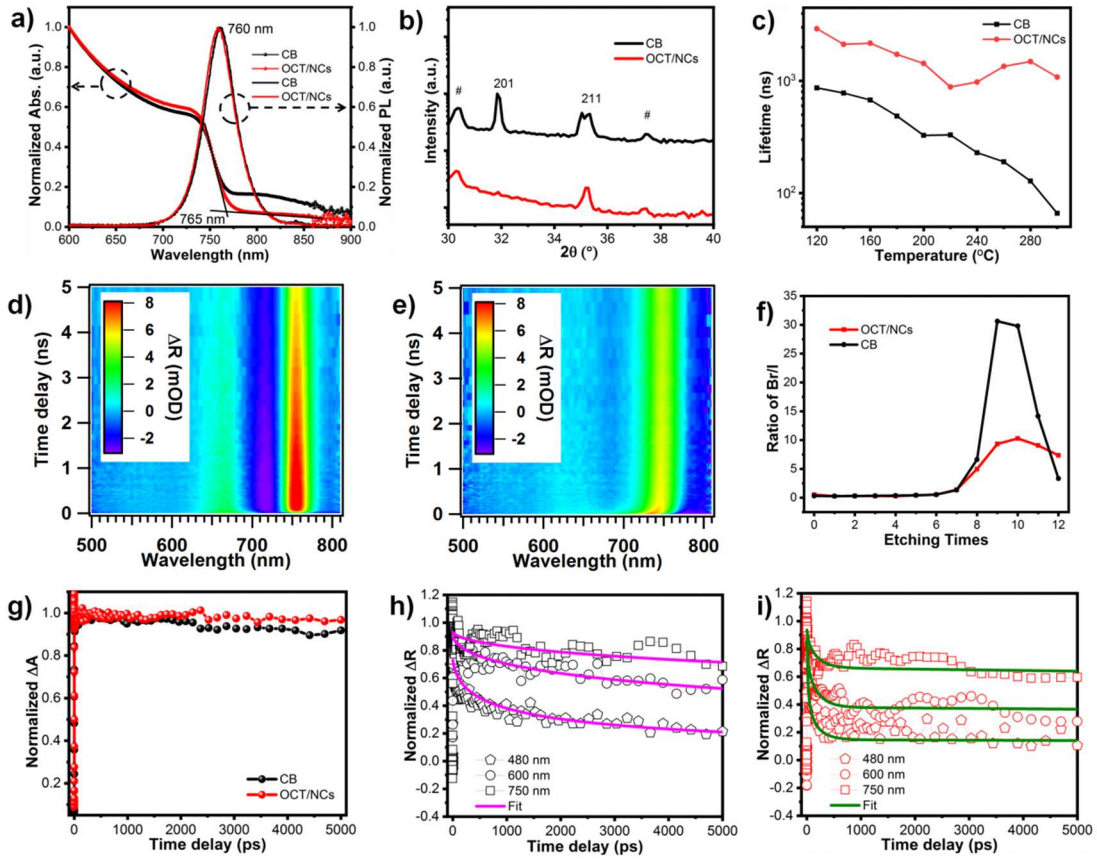

Fig. 5 | Optoelectronic properties characterization. a, UV-vis spectra and PL spectra of CB and OCT/NCs processed perovskite films. **b,** Diffraction split of (211) facet in XRD pattern for CB processed perovskite film. (#: ITO). **c,** TRPL lifetime dependent on different temperature. **d,e,** TA spectra of perovskite films processed by (**d**) CB and (**e**) OCT/NCs from glass side. **f,** Variation of Br^-/I^- atom ratio by XPS with different etching times. **g,** Ultrafast carrier kinetics of perovskite films by TA . **h,i,** Ultrafast carrier kinetics of perovskite/NiO interface processed by (**h**) CB and (**i**) OCT/NCs by TR spectra excited by lasers with wavelength of 480 nm, 600 nm and 750 nm from glass side.

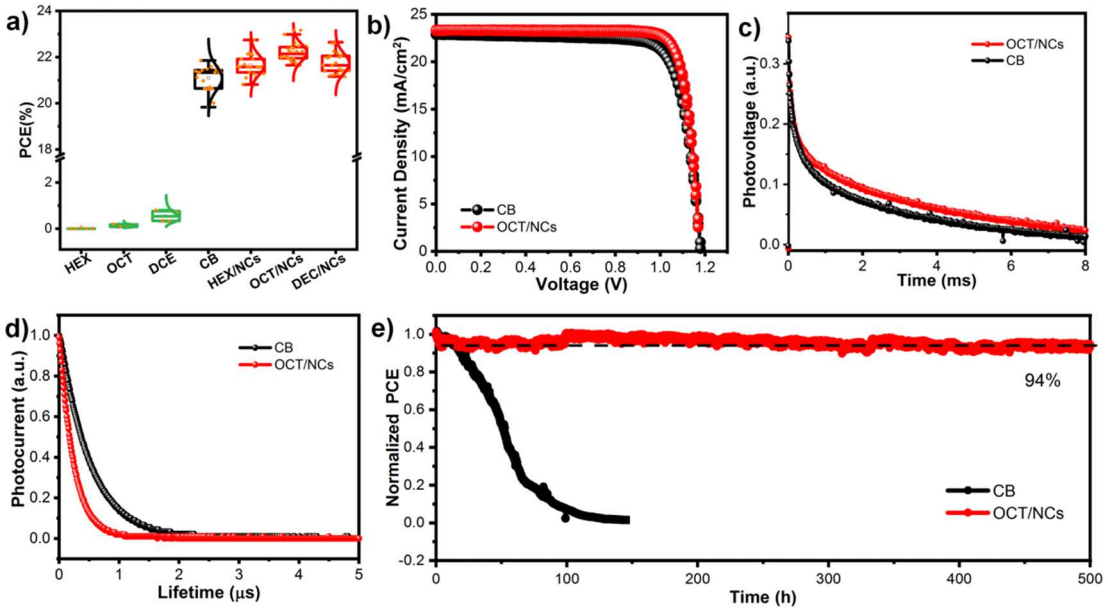

Fig. 6 | Devices characterization. a, PCE distribution of devices fabricated by different kinds of anti-solvents. **b,** J-V curve of champion devices fabricated by CB and OCT/NCs. **c,** Transient photovoltage decay. **d,** Transient photocurrent decay. **e,** MPPT curve of light soaking test of enacapusulated devices in air atmosphere.